Pinwheel-like Curved Aromatics from the Cyclotrimerization of Strained Alkyne Cycloparaphenylenes

Julia M. Fehr[a], Tara D. Clayton[a], Tavis W. Price[a], Lev N. Zakharov[b], and Ramesh Jasti[a]*

[a] Department of Chemistry and Biochemistry, Materials Science Institute, and Knight Campus for Accelerating Scientific Impact, University of Oregon, Eugene, Oregon 97403, USA. *Email: rjasti@uoregon.edu.
[b] CAMCOR – Center for Advanced Materials Characterization in Oregon, University of Oregon, Eugene, Oregon, 97403, USA.

ABSTRACT: Curved aromatic hydrocarbons often display better solubility and more desirable electronic properties in comparison to their flat counterparts. Macrocyclic curved aromatics possess these traits as well as shape-persistent pores ideal for host-guest interactions. A quintessential macrocyclic curved aromatic molecule is the cycloparaphenylene, or [*n*]CPP. Our group has developed a new class of these carbon nanohoops, called [*n*+1]CPPs, that incorporate a strained alkyne ("+1") into the carbon backbone. We have previously shown the [*n*+1]CPPs to be a promising new class of strain-promoted azide-alkyne cycloaddition click reagents. Herein, we show that the [*n*+1]CPPs can also be converted into pinwheel-like multi-pore large molecules *via* a straightforward and high yielding metal-mediated alkyne cyclotrimerization reaction. We provide insight into suitable metals for this transformation, the photophysics of these trimeric molecules, as well as their strain profiles and crystal packing.

INTRODUCTION

Curved aromatic hydrocarbons are a useful and continuously evolving class of carbon nanomaterials. Their deviation from the flat, planar topology expected of aromatic molecules can grant them advantages such as: (1) narrower HOMO-LUMO gaps with increasing strain,[1] (2) heightened solubility due to less efficient self-stacking,[2] and (3) complementary intermolecular interactions such as convex-concave π-interactions.[3,4] Since the landmark discoveries of fullerenes and carbon nanotubes,[5,6] many molecular topologies of curved aromatic hydrocarbons have been synthesized. Small

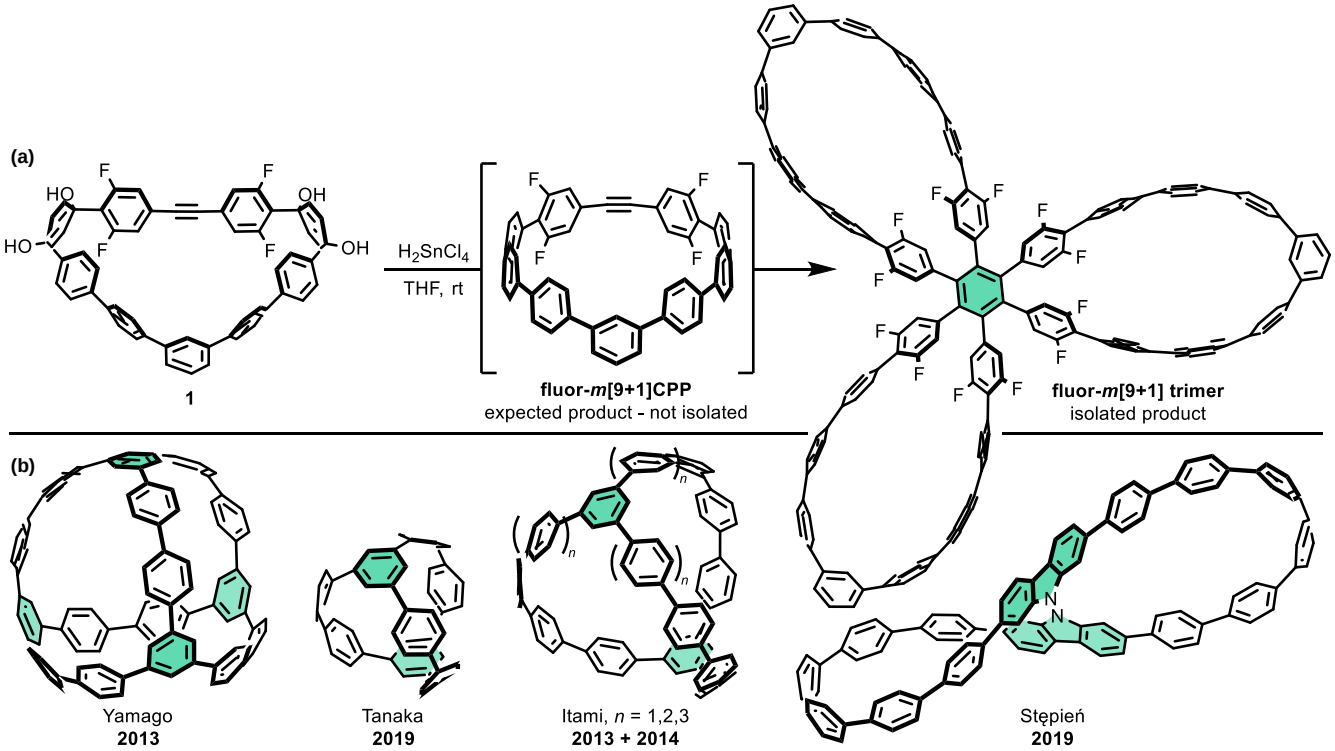

Figure 1. (a) Initial findings wherein subjection of macrocycle **1** to reductive aromatization conditions resulted not in isolation of the expected strained alkyne-containing **fluor-*m*[9+1]CPP** but instead **fluor-*m*[9+1] trimer**. (b) Previous examples of multi-pore nanohoop-type structures.

molecules such as helicenes, corannulenes, saddle-shaped polyaromatics, and a variety of conjugated macrocycles are now accessible *via* controlled, bottom-up synthetic methods.[7]

Specifically, macrocycles in this class combine the attractive properties of curved aromatics with the added benefits of shape-persistent pores and host-guest capabilities.[3,4] Carbon nanohoops (also known as cycloparaphenylenes and abbreviated [*n*]CPP where *n* = number of phenylene units) are strained aromatic macrocycles that represent the smallest cross-section of an armchair carbon nanotube.[8] In the last several years, carbon nanohoops have garnered much attention from the broader scientific community.[7,9–14] Many molecules in this class are redox active,[14–18] brightly fluorescent,[15] possess excellent solubility in most organic solvents,[15] and have syntheses which are highly modular and tunable; this allows for the study of nanohoops of many different sizes, shapes, functionalities, and properties.[7,9–14,19]

One such variation is alkyne-inserted [*n*]CPPs that incorporate one or more strained carbon-carbon triple bond into the backbone of the macrocycle. The synthesis of such molecules was first accomplished[20] by Kawase *et al.* in 1996 and is still of interest today,[21–23] particularly due to the ability for alkyne-inserted [*n*]CPPs to react further at controlled sites on the molecule, for instance *via* the strain-promoted azide-alkyne cycloaddition (SPAAC). Our group has recently focused on the synthesis and study of [*n*+1]CPPs,[24] wherein the "+1" refers to the incorporation of a single alkyne inserted in the macrocyclic backbone. These molecules have tunable reactivity towards the SPAAC reaction,[24,25] and we have also shown that one iteration, **[11+1]CPP**, is converted to a lasso-shaped molecule capable of hosting C_{60} and C_{70} post-click reaction.[26]

Our most recent work focused on heightening [*n*+1]CPP reactivity by (1) the introduction of electron-withdrawing fluorine atoms near the strained alkyne, and (2) the installation of a *meta*-linked phenylene into the nanohoop opposite the alkyne.[25] While working to synthesize even more strained and electronically activated [*n*+1]CPPs, namely **fluor-*m*[9+1]CPP** (**Figure 1a**), we observed a byproduct of the final reductive aromatization of precursor **1** with the same symmetry as the desired carbon nanohoop but lacking characteristic alkyne ^{13}C signals and any reactivity towards azides. Further investigation of this byproduct revealed it to be a pinwheel-like molecule produced by alkyne cyclotrimerization involving three [*n*+1]CPPs (**fluor-*m*[9+1] trimer**, **Figure 1a**). Herein, we describe our efforts to better understand the formation of [*n*+1] trimers and their physical properties. These new molecules possess three shape-persistent pores, and mark the next installment to a class of carbon nanohoop derivatives with multiple shape-persistent openings (**Figure 1b**).[27–31]

RESULTS AND DISCUSSION

Our isolation of **fluor-*m*[9+1] trimer** instead of our original target molecule **fluor-*m*[9+1]CPP** motivated us to synthesize a similar but slightly less reactive [*n*+1]CPP as a point of comparison. We therefore focused our attention on the synthesis of the fully *para*-linked **fluor[9+1]CPP** (**Scheme 1**) using a combination of previously described[24,25] molecular building blocks (see SI for full synthetic details). We found that **fluor[9+1]CPP** could be isolated effectively under the same reaction and purification conditions which had proved unsuccessful for **fluor-*m*[9+1]CPP**. Interestingly, we would occasionally observe slow conversion of **fluor[9+1]CPP** to **fluor[9+1] trimer** if the sample was kept as a solution in previously used glassware and/or had not yet been rigorously purified; this led us to hypothesize that the trimerization might be catalyzed by metal impurities.

With the comparatively more stable **fluor[9+1]CPP** in hand, we turned our attention to better understanding the nature of the trimerization reaction. Under inert atmosphere at room temperature with freshly clean glassware in deuterated chloroform ($CDCl_3$), we treated **fluor[9+1]CPP** with a metal catalyst (approximately 20% catalyst loading) for one hour and assessed the results of each reaction with quantitative ^{19}F NMR (**Table 1** and **Scheme 1**). The screened metals are well-known catalysts for alkyne trimerization; Rh(I)[32,33] and Ni(0)[34–36] are common catalysts for the trimerization of unstrained alkynes, while Pd(0)[37–39] is often an effective catalyst for aryne trimerization.

Table 1. Metal screening results for conversion of **fluor[9+1]CPP** to **fluor[9+1] trimer**.

metal	conversion (%)
none	0.5
$Pd_2(dba)_3$	99.9
$RhCl(PPh_3)_3$	6.3
Ni(cod)DQ	11.5

Reactions carried out in $CDCl_3$ at room temperature for 1 h under inert atmosphere with 1.9 mM **fluor[9+1]CPP**, 0.39 mM metal. Conversions determined by quantitative ^{19}F NMR.

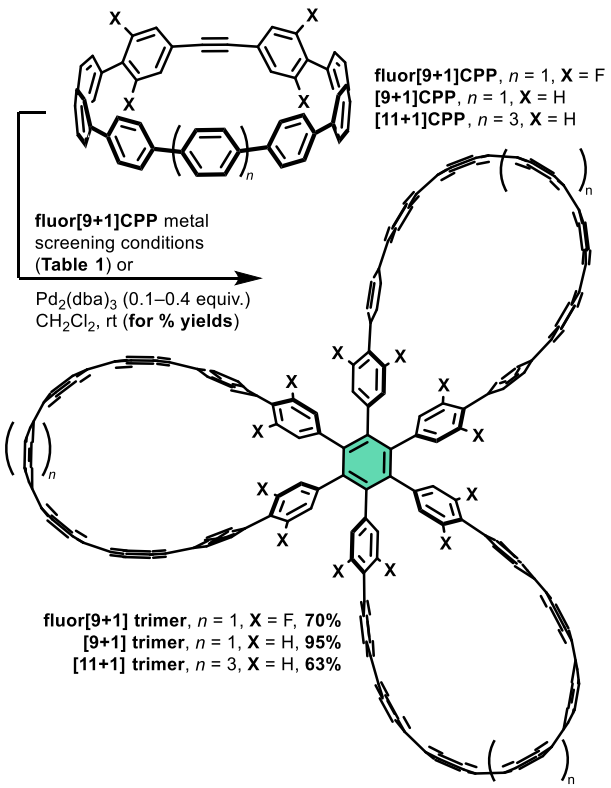

Scheme 1. Conversion of [*n*+1]CPPs to trimers. **Fluor[9+1]CPP** was chosen as a model system to assess the effectiveness of metal catalysts on the reaction (see **Table 1**). Percent yields refer to optimized conditions with $Pd_2(dba)_3$.

We found that $Pd_2(dba)_3$ was by far the most efficient catalyst for the transformation of **fluor[9+1]CPP** to **fluor[9+1] trimer**, with a calculated percent conversion of over 99% (with these conditions, we achieved 70% isolated yield in a separate experiment). $RhCl(PPh_3)_3$ and Ni(cod)DQ performed much more modestly at 6.3% and 11.5% conversion, respectively. We were surprised by these results as they suggest that the reactivity of [*n*+1]CPPs more closely resembles that of benzyne rather than unstrained alkynes. Notably, with highly pure **fluor[9+1]CPP** starting material in clean glassware (first entry of **Table 1**), we saw less than 0.5% conversion to **fluor[9+1] trimer** in our hour-long, room temperature control experiment with no added metal. In a separate control experiment, we found that diphenylacetylene (an unstrained, phenyl-substituted alkyne) showed no reaction under the same conditions with $Pd_2(dba)_3$ (see SI for details).

We next questioned whether less reactive [*n*+1]CPPs could undergo cyclotrimerization under the same conditions. To assess whether electron-withdrawing fluorine atoms were necessary for the transformation, we combined **[9+1]CPP** and catalytic $Pd_2(dba)_3$ and found that alkyne cyclotrimerization occurred efficiently to form **[9+1] trimer** in 95% isolated yield. To investigate if less strained [*n*+1]CPPs were also capable of this transformation, we subsequently treated **[11+1]CPP** with $Pd_2(dba)_3$ and found that **[11+1] trimer** could be isolated in 63% yield. While we found that **[9+1] trimer**, **fluor[9+1] trimer**, and **fluor-*m*[9+1] trimer** all possessed excellent solubility in a range of organic solvents, **[11+1] trimer** suffered from a lack of significant solubility in most solvents, which likely contributed to its diminished isolated yield.

Finally, we turned our attention back to a more efficient synthesis of **fluor-*m*[9+1] trimer**. After testing several methods, we found that we could reliably form **fluor-*m*[9+1] trimer** by adding 1.5 equivalents of Ni(cod)DQ directly to the reductive aromatization reaction of **fluor-*m*[9+1]CPP**. This allowed us to form **fluor-*m*[9+1] trimer** in up to 52% yield from **1** after purification.

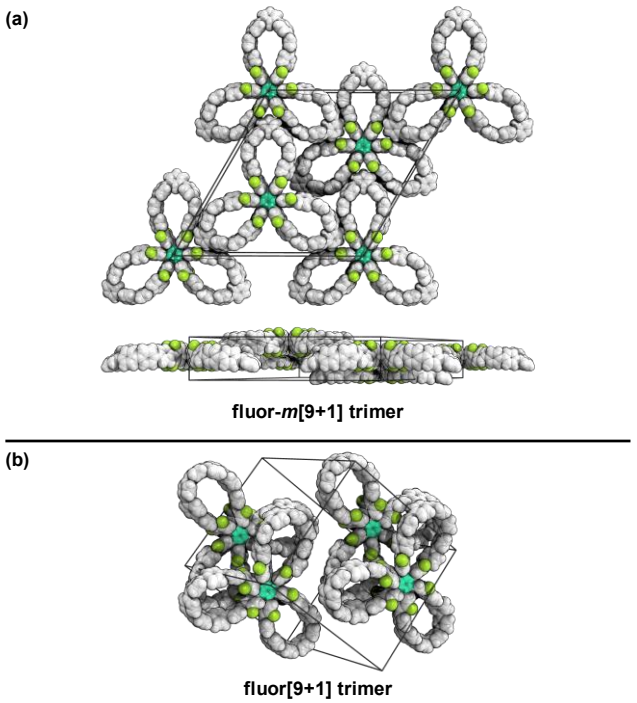

Figure 2. X-ray crystal structure unit cells of (a) **fluor-*m*[9+1] trimer** and (b) **fluor[9+1] trimer**. Solvent omitted for clarity.

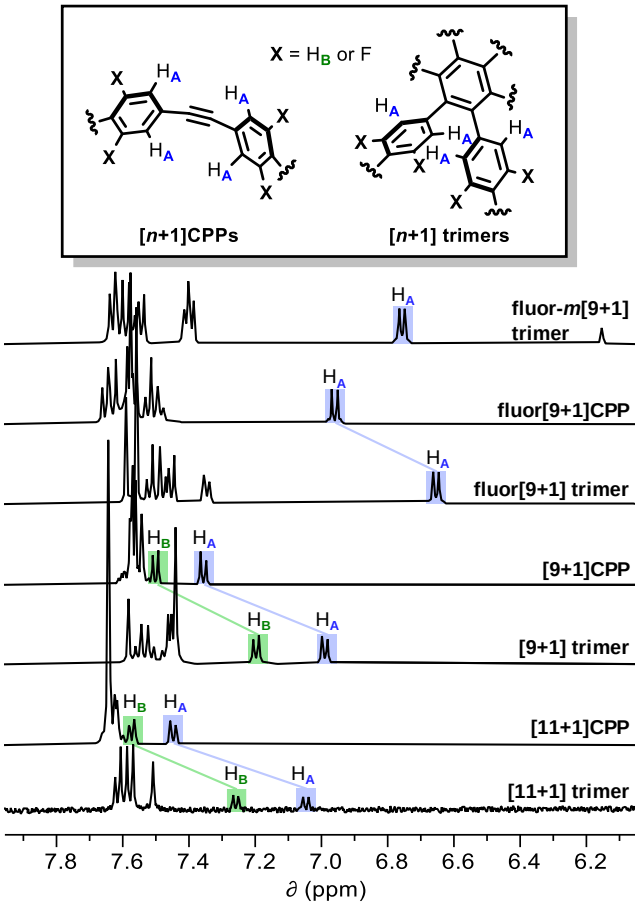

Figure 3. Diagnostic ^1H NMR shifts for trimers and associated [*n*+1]CPPs in CD_2Cl_2.

We confirmed the identity and connectivity of **fluor-*m*[9+1] trimer** and **fluor[9+1] trimer** *via* X-ray crystal analysis (unit cells shown in **Figure 2**). Crystals of **fluor[9+1] trimer** were formed from the slow evaporation of 1,4-dioxane. Crystals of **fluor-*m*[9+1] trimer** were formed from vapor diffusion of pentanes into 1,4-dioxane. In both cases, precise structural information could not be determined due to a high number of disordered solvent molecules. However, the X-ray data was sufficient to confirm the correct assignment of both molecules and assign a space group (*P* -1 for **fluor[9+1] trimer** and *R* 3 for **fluor-*m*[9+1] trimer**) for each crystal packing pattern. Notably, **fluor-*m*[9+1] trimer** packs into an interdigitated structure with long-range, solvent-filled channels.

While we were not able to grow suitable single crystals of **[9+1] trimer** and **[11+1] trimer**, spectroscopic evidence is indicative of their successful synthesis. **Figure 3** shows the ^1H NMR spectra in deuterated dichloromethane (CD_2Cl_2) for each of the trimers described herein as well as relevant [*n*+1]CPPs. For [*n*+1]CPPs, we typically observe a distinctive upfield doublet representative of the hydrogens *ortho* to the alkyne (shown generically as H_A in **Figure 3**).[24,25] For non-fluorinated **[9+1]CPP** and **[11+1]CPP**, another upfield doublet, likely representative of the hydrogens *meta* to the alkyne (H_B in **Figure 3**), can also be observed. Upon trimerization of **fluor[9+1]CPP**, an upfield shift of the H_A

doublet occurred from 6.96 ([*n*+1]CPP) to 6.65 ppm (trimer). Notably, the H_A doublets of **[9+1]CPP** and **[11+1]CPP** experience very comparable shifts upon trimerization (7.36 to 6.99 ppm for **[9+1]CPP** to **[9+1] trimer**, and 7.45 to 7.05 ppm for **[11+1]CPP** to **[11+1] trimer**). In these cases, we can also note the upfield shift of the H_B signal; the doublet representing H_B shifts from 7.50 ppm for **[9+1]CPP** to 7.20 ppm for **[9+1] trimer**, and from 7.57 ppm for **[11+1]CPP** to 7.26 ppm for **[11+1] trimer**.

Further NMR evidence for successful trimerization can be found in the ^{13}C NMR (see SI for full details). In these spectra, we see a disappearance of any signals below 120 ppm, indicating the lack of an alkyne in the product (the alkyne signals for **fluor[9+1]CPP**, **[9+1]CPP**, and **[11+1]CPP** in CD_2Cl_2 are observed at 99.24 ppm, 99.39 ppm, and 97.10 ppm, respectively). In addition to spectroscopic evidence, high resolution mass spectrometry of **fluor-*m*[9+1] trimer**, **fluor[9+1] trimer**, **[9+1] trimer**, and **[11+1] trimer** resulted in the correct ion masses.

We next worked to better understand the total strain and distribution of local strain in these new nanohoop derivatives. We used the computational program StrainViz to calculate and visualize the local and total strain of each trimer and its parent [*n*+1]CPP (**Table 2** and **Figure 4**).[40] For the [*n*+1]CPPs, local strain is greatest at the alkyne as has been shown previously.[25,40] For the trimers, however, local strain is greatest at the phenylene units opposite the newly formed *ortho* linkage—this is consistent with our understanding of how strain is distributed in these types of macrocycles.[40] Additionally, the trimers have total strain values equivalent to less than three times the total strain of the precursor [*n*+1]CPPs. For example, **fluor[9+1] trimer** has a calculated 130 kcal mol^{-1} of inherent strain, whereas **fluor[9+1]CPP** has 56 kcal mol^{-1}. These findings indicate that the inherent strain per macrocyclic unit decreases post-trimerization. We also

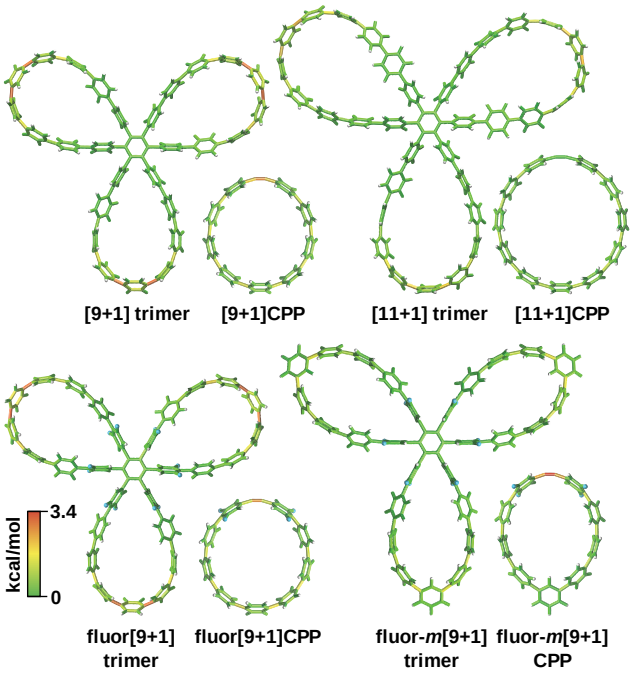

Figure 4. StrainViz structures for each trimer and its respective [*n*+1]CPP (**fluor-*m*[9+1]CPP** was not isolated but is shown here for completeness).

note that **fluor-*m*[9+1]CPP**, which has the highest calculated maximum local strain value of the [*n*+1]CPPs in this study at 3.4 kcal mol^{-1}, trimerizes to form the most locally and globally unstrained trimer in this series, **fluor-*m*[9+1] trimer**. The *meta* linkage serves to heighten strain in nanohoops at the region of the molecule directly across from it,[40] but post-trimerization the newly formed *ortho*-linkage ameliorates this effect.

Table 2. Quantitative strain data as determined by StrainViz (all values in kcal mol^{-1}). Computations performed with Gaussian 09 at the B3LYP/6-31G(d) level of theory.

compound	max. local strain	total strain
fluor-*m*[9+1] trimer	1.8	80.5
fluor[9+1] trimer	3.1	130.3
[9+1] trimer	3.1	129.3
[11+1] trimer	2.3	112.8
fluor-*m*[9+1]CPP	3.4	42.9
fluor[9+1]CPP	2.8	55.6
[9+1]CPP	2.9	58.0
[11+1]CPP	1.3	44.4

Photophysical data for each trimer and its associated parent [*n*+1]CPP[24,25] (where applicable) are displayed in **Figure 5** and **Table 3**. Absorbance and emission traces as well as quantum yields were collected for all molecules in comparatively nonpolar dichloromethane (DCM) and polar dimethyl sulfoxide (DMSO) to understand any solvent-dependent effects; extinction coefficients were collected in DCM. For all trimers, we did not observe a large solvent effect on photophysics beyond a slight red-shifting in maximum absorbance wavelength ($\lambda_{max,abs}$) and maximum emission wavelength ($\lambda_{max,em}$) values in DMSO (**Table 3** and **Figure 5c**). Therefore, we will focus our analysis of trimer photophysics on the measured values in DCM. The only notable solvent effects were observed for **fluor[9+1]CPP**, which displayed highly solvent-dependent fluorescence properties (*vide infra*).

In most carbon nanohoops, we observe a $\lambda_{max,abs}$ around 340 nm. This major absorbance band is dominated by degenerate HOMO-2/HOMO-1 to LUMO and HOMO to LUMO+1/LUMO+2 transitions, as the HOMO to LUMO transition is symmetry forbidden in most cases.[15,41] Fluorescence profiles in carbon nanohoops generally occurs by emission from a localized excited state (S_1') down to the ground state S_0; the energy of this transition is dictated by the size of the HOMO-LUMO gap.[15,41] These general trends have been observed previously for many nanohoop derivatives, including [*n*+1]CPPs.[24,25]

When comparing the absorbance profiles of each trimer to its parent [*n*+1]CPP, we can observe a slight hypsochromic shift of $\lambda_{max,abs}$ upon trimerization. For example, **[9+1]CPP** has a measured $\lambda_{max,abs}$ of 342 nm in DCM, while **[9+1] trimer** has a slightly blue-shifted $\lambda_{max,abs}$ of 337 nm. Nonetheless, **fluor[9+1] trimer**, **[9+1] trimer**, and **[11+1] trimer** all maintain $\lambda_{max,abs}$ values around the typical 340 nm. Comparing the trimers, we note that **fluor[9+1] trimer** has a slightly blue-shifted $\lambda_{max,abs}$ compared to **[9+1] trimer**. We have previously observed a slight hypsochromic shift in fluorinated *para*-linked nanohoops compared to their hydrocarbon counterparts.[25,42,43] Finally, the shortest wavelength $\lambda_{max,abs}$ is displayed by **fluor-*m*[9+1] trimer**; we hypothesize that the significant lack of strain in this molecule

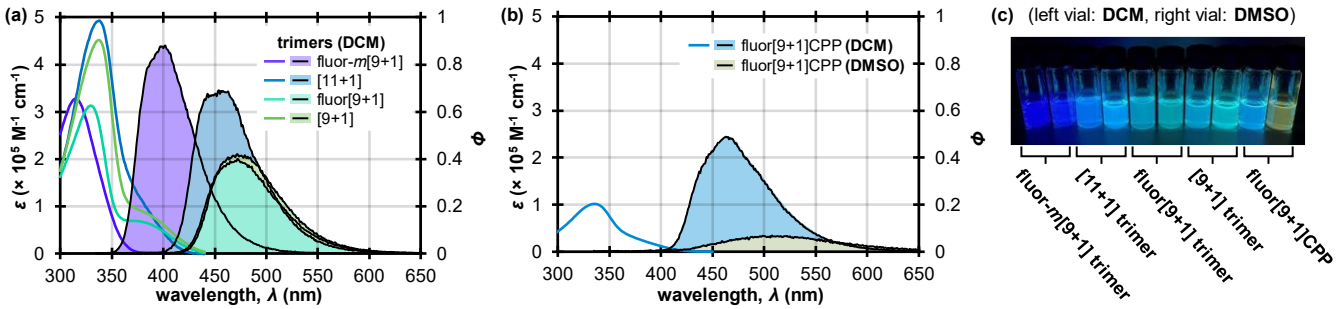

Figure 5. Photophysical characterization for the new molecules described herein. (a) Extinction coefficients (colored lines) and fluorescence emission traces (black lines) for each trimer in DCM plotted as a function of wavelength. Fluorescence traces are scaled such that the maximum *y*-value of each curve matches the quantum yield of the compound in DCM. (b) Extinction coefficient for **fluor[9+1]CPP** (blue line) as a function of wavelength in DCM plotted along with fluorescence emission traces (black lines) for **fluor[9+1]CPP** in DCM and DMSO (emission curves are also scaled to quantum yield in the respective solvent). (c) Solutions of trimers and **fluor[9+1]CPP** in DCM and DMSO under irradiation with long-wave UV light.

Table 3. Tabulated photophysical data for trimers and associated [*n*+1]CPPs.

compound	$\lambda_{max,abs}$ (nm)		$\lambda_{max,em}$ (nm)		extinction coefficient, ε (× 10^5 M^{-1} cm^{-1})	quantum yield, Φ	
	DCM	DMSO	DCM	DMSO	DCM	DCM	DMSO
fluor-*m*[9+1] trimer	315	318	402	415	3.27 ± 0.04	0.88	0.88
fluor[9+1] trimer	330	337	472	479	3.13 ± 0.23	0.40	0.46
[9+1] trimer	337	344	472	487	4.52 ± 0.07	0.42	0.47
[11+1] trimer	338	345	454	468	4.93 ± 0.20	0.69	0.67
fluor[9+1]CPP	335	343	463	507	1.02 ± 0.04	0.49	0.07
[9+1]CPP	342	351	463	473	1.55	0.76	0.67
[11+1]CPP	341	350	449	460	1.63	0.80	0.83

* values for **[9+1]CPP** and **[11+1]CPP** were measured previously[24,25] and included here as a point of reference. Note that quantum yields were measured by slightly different methods than were used in this study (see SI and previous publications for details).

in comparison to the other trimers elevates the energy of this transition.[44]

The extinction coefficient for each trimer is plotted as a function of wavelength in **Figure 5a**; extinction coefficients for each trimer (and corresponding [*n*+1]CPP) at $\lambda_{max,abs}$ are displayed in **Table 3**. In each case where it is possible to compare the trimer to its [*n*+1]CPP parent, we observe that the extinction coefficient at $\lambda_{max,abs}$ is (within error) approximately three times that of the parent. For instance, we previously measured an extinction coefficient for **[9+1]CPP** of 1.55 × 10^5 M^{-1} cm^{-1} in DCM at $\lambda_{max,abs}$.[24] This value essentially triples for **[9+1] trimer** with a measured extinction coefficient of 4.52 × 10^5 M^{-1} cm^{-1}. This is an intriguing result which suggests that the molar absorptivity of each [*n*+1]CPP macrocycle is maintained even upon its incorporation into the trimeric species, establishing the [*n*+1] trimers as exceptionally bright chromophores.

The fluorescence emission traces for each trimer are plotted in **Figure 5a** as a function of wavelength and normalized such that the maximum *y*-axis value matches the molecule's measured quantum yield in DCM. We observe that **[11+1] trimer**, **fluor[9+1] trimer**, and **[9+1] trimer** display fluorescence emissions that are slightly red-shifted in comparison to their parent [*n*+1]CPPs; for example, the maximum emission wavelength ($\lambda_{max,em}$) for **[9+1]CPP** in DCM was previously measured to be 463 nm,[24] while **[9+1] trimer** displays a $\lambda_{max,em}$ of 472 nm. As is generally observed in carbon nanohoops,[15] the smaller **[9+1] trimer** and **fluor[9+1] trimer** have a red-shifted emission in comparison to the larger **[11+1] trimer**, probably due to heightened conjugation between phenylenes in smaller sizes. We observe that fluorination of the **[9+1] trimer** scaffold does not seem to significantly affect fluorescence properties. The hypsochromic fluorescence emission of **fluor-*m*[9+1] trimer** in comparison to the other trimers in this study can most likely be attributed to a lack of strain in the molecule which in turn decreases p-orbital overlap and widens the HOMO-LUMO gap.[15,44] Quantum yields for all trimers were reasonably high: **fluor[9+1] trimer** and **[9+1] trimer** displayed quantum yields of 0.40 and 0.42 in DCM, respectively, while the larger **[11+1] trimer** displayed a slightly higher quantum yield of 0.69. **Fluor-*m*[9+1] trimer** exhibited the highest quantum yield in the series at 0.88.

Figure 5b and **5c** highlight the significant solvent-dependent fluorescence properties of **fluor[9+1]CPP**. The $\lambda_{max,em}$ for **fluor[9+1]CPP** shifts from 463 nm in DCM to 507 nm in DMSO. This bathochromic shift in $\lambda_{max,em}$ with increasing solvent polarity is accompanied by a notable drop in quantum yield from 0.49 in DCM to 0.07 in DMSO. These results suggest that **fluor[9+1]CPP** is a new donor-acceptor-type nanohoop that, upon excitation, experiences charge transfer from the electron-rich curved phenylene backbone of the nanohoop to the electron-poor, fluorinated, alkyne-containing region.[14,16,17,25,45–48] We speculate that a polarized excited state would be better stabilized in polar solvents such as DMSO, therefore resulting in a lower energy transition back to the ground state and longer wavelength $\lambda_{max,em}$.[49] The lower quantum yield would in turn be explained by the energy gap law, as has been seen previously for donor-acceptor molecules.[50] The fact that the quantum yield in DMSO is largely restored upon trimerization to **fluor[9+1] trimer** suggests that the trimer's excited state is significantly less polarized.[49,50]

CONCLUSION

Our previous studies of strained alkyne carbon nanohoops focused on efficiently attaching them *via* click chemistry methods to other molecules of interest.[24–26] Herein, we have described a synthetically simple and high yielding method for derivatizing these molecules further by a metal-catalyzed trimerization reaction. The result is high molecular weight pinwheel-shaped [*n*+1] trimers that maintain nanohoop-type photophysics and generally good solubility. We envision that this method can provide access to trimer derivatives with unique photophysics, topology, and functionality, especially given the modularity of most [*n*+1]CPP syntheses. This finding also provides further evidence that strained alkyne nanohoops are amenable to derivatization through a variety of pathways, and we look forward to exploring this further in future work.

ACKNOWLEDGEMENTS

We would like to acknowledge the National Science Foundation (NSF) grant number NSF-CHE-2102567. This work benefited from the Oregon high performance computer, Talapas.

REFERENCES

(1) Scott, L. T.; Bronstein, H. E.; Preda, D. V.; Ansems, R. B. M.; Bratcher, M. S.; Hagen, S. Geodesic Polyarenes with Exposed Concave Surfaces. *Pure Appl. Chem.* **1999**, *71*, 209–219.

(2) Bheemireddy, S. R.; Ubaldo, P. C.; Finke, A. D.; Wang, L.; Plunkett, K. N. Contorted Aromatics via a Palladium-Catalyzed Cyclopentannulation Strategy. *J. Mater. Chem. C* **2016**, *4*, 3963–3969.

(3) Xu, Y.; Kaur, R.; Wang, B.; Minameyer, M. B.; Gsänger, S.; Meyer, B.; Drewello, T.; Guldi, D. M.; von Delius, M. Concave–Convex π–π Template Approach Enables the Synthesis of [10]Cycloparaphenylene–Fullerene [2]Rotaxanes. *J. Am. Chem. Soc.* **2018**, *140*, 13413–13420.

(4) Ball, M.; Zhong, Y.; Fowler, B.; Zhang, B.; Li, P.; Etkin, G.; Paley, D. W.; Decatur, J.; Dalsania, A. K.; Li, H.; Xiao, S.; Ng, F.; Steigerwald, M. L.; Nuckolls, C. Macrocyclization in the Design of Organic N-Type Electronic Materials. *J. Am. Chem. Soc.* **2016**, *138*, 12861–12867.

(5) Iijima, S. Helical Microtubules of Graphitic Carbon. *Nature* **1991**, *354*, 56–58.

(6) Kroto, H. W.; Heath, J. R.; O'Brien, S. C.; Curl, R. F.; Smalley, R. E. C60: Buckminsterfullerene. *Nature* **1985**, *318*, 162–163.

(7) Majewski, M. A.; Stępień, M. Bowls, Hoops, and Saddles: Synthetic Approaches to Curved Aromatic Molecules. *Angew. Chem. Int. Ed.* **2019**, *58*, 86–116.

(8) Jasti, R.; Bhattacharjee, J.; Neaton, J. B.; Bertozzi, C. R. Synthesis, Characterization, and Theory of [9]-, [12]-, and [18]Cycloparaphenylene: Carbon Nanohoop Structures. *J. Am. Chem. Soc.* **2008**, *130*, 17646–17647.

(9) Lewis, S. E. Cycloparaphenylenes and Related Nanohoops. *Chem. Soc. Rev.* **2015**, *44*, 2221–2304.

(10) Wu, D.; Cheng, W.; Ban, X.; Xia, J. Cycloparaphenylenes (CPPs): An Overview of Synthesis, Properties, and Potential Applications. *Asian J. Org. Chem.* **2018**, *7*, 2161–2181.

(11) Yamago, S.; Kayahara, E. Synthesis and Reactions of Carbon Nanohoop. *J. Synth. Org. Chem. Jpn.* **2019**, *77*, 1147–1158.

(12) Xu, Y.; von Delius, M. The Supramolecular Chemistry of Strained Carbon Nanohoops. *Angew. Chem. Int. Ed.* **2020**, *59*, 559–573.

(13) Li, Y.; Kono, H.; Maekawa, T.; Segawa, Y.; Yagi, A.; Itami, K. Chemical Synthesis of Carbon Nanorings and Nanobelts. *Acc. Mater. Res.* **2021**, *2*, 681–691.

(14) Hermann, M.; Wassy, D.; Esser, B. Conjugated Nanohoops Incorporating Donor, Acceptor, Hetero- or Polycyclic Aromatics. *Angew. Chem. Int. Ed.* **2021**, *60*, 15743–15766.

(15) Darzi, E. R.; Jasti, R. The Dynamic, Size-Dependent Properties of [5]–[12]Cycloparaphenylenes. *Chem. Soc. Rev.* **2015**, *44*, 6401–6410.

(16) Darzi, E. R.; Hirst, E. S.; Weber, C. D.; Zakharov, L. N.; Lonergan, M. C.; Jasti, R. Synthesis, Properties, and Design Principles of Donor–Acceptor Nanohoops. *ACS Cent. Sci.* **2015**, *1*, 335–342.

(17) Van Raden, J. M.; Darzi, E. R.; Zakharov, L. N.; Jasti, R. Synthesis and Characterization of a Highly Strained Donor–Acceptor Nanohoop. *Org. Biomol. Chem.* **2016**, *14*, 5721–5727.

(18) Narita, N.; Kurita, Y.; Osakada, K.; Ide, T.; Kawai, H.; Tsuchido, Y. A Dodecamethoxy[6]Cycloparaphenylene Consisting Entirely of Hydroquinone Ethers: Unveiling in-Plane Aromaticity through a Rotaxane Structure. *Nat. Commun.* **2023**, *14*, 8091.

(19) Leonhardt, E. J.; Jasti, R. Emerging Applications of Carbon Nanohoops. *Nat. Rev. Chem.* **2019**, *3*, 672–686.

(20) Kawase, T.; Darabi, H. R.; Oda, M. Cyclic [6]- and [8]Paraphenylacetylenes. *Angew. Chem. Int. Ed. Engl.* **1996**, *35*, 2664–2666.

(21) Lee, S.; Chénard, E.; Gray, D. L.; Moore, J. S. Synthesis of Cycloparaphenyleneacetylene via Alkyne Metathesis: C $_{70}$ Complexation and Copper-Free Triple Click Reaction. *J. Am. Chem. Soc.* **2016**, *138*, 13814–13817.

(22) Zhou, X.; Thompson, R. R.; Fronczek, F. R.; Lee, S. Size-Selective Synthesis of Large Cycloparaphenyleneacetylene Carbon Nanohoops Using Alkyne Metathesis. *Org. Lett.* **2019**, *21*, 4680–4683.

(23) Zhou, X.; Kwon, H.; Thompson, R. R.; Herman, R. J.; Fronczek, F. R.; Bruns, C. J.; Lee, S. Scalable Synthesis of [8]Cycloparaphenyleneacetylene Carbon Nanohoop Using Alkyne Metathesis. *Chem. Commun.* **2021**, *57*, 10887–10890.

(24) Schaub, T. A.; Margraf, J. T.; Zakharov, L.; Reuter, K.; Jasti, R. Strain-Promoted Reactivity of Alkyne-Containing Cycloparaphenylenes. *Angew. Chem. Int. Ed.* **2018**, *57*, 16348–16353.

(25) Fehr, J. M.; Myrthil, N.; Garrison, A. L.; Price, T. W.; Lopez, S. A.; Jasti, R. Experimental and Theoretical Elucidation of SPAAC Kinetics for Strained Alkyne-Containing Cycloparaphenylenes. *Chem. Sci.* **2023**, *14*, 2839–2848.

(26) Schaub, T. A.; Zieleniewska, A.; Kaur, R.; Minameyer, M.; Yang, W.; Schüßlbauer, C. M.; Zhang, L.; Freiberger, M.; Zakharov, L. N.; Drewello, T.; Dral, P. O.; Guldi, D. M.; Jasti, R. Tunable Macrocyclic Polyparaphenylene Nanolassos via Copper-Free Click Chemistry. *Chem. Eur. J.* **2023**, *29*, e202300668.

(27) Kayahara, E.; Iwamoto, T.; Takaya, H.; Suzuki, T.; Fujitsuka, M.; Majima, T.; Yasuda, N.; Matsuyama, N.; Seki, S.; Yamago, S. Synthesis and Physical

Properties of a Ball-like Three-Dimensional π-Conjugated Molecule. *Nat. Commun.* **2013**, *4*, 2694.
(28) Hayase, N.; Nogami, J.; Shibata, Y.; Tanaka, K. Synthesis of a Strained Spherical Carbon Nanocage by Regioselective Alkyne Cyclotrimerization. *Angew. Chem. Int. Ed.* **2019**, *58*, 9439–9442.
(29) Matsui, K.; Segawa, Y.; Namikawa, T.; Kamada, K.; Itami, K. Synthesis and Properties of All-Benzene Carbon Nanocages: A Junction Unit of Branched Carbon Nanotubes. *Chem. Sci.* **2012**, *4*, 84–88.
(30) Matsui, K.; Segawa, Y.; Itami, K. All-Benzene Carbon Nanocages: Size-Selective Synthesis, Photophysical Properties, and Crystal Structure. *J. Am. Chem. Soc.* **2014**, *136*, 16452–16458.
(31) Senthilkumar, K.; Kondratowicz, M.; Lis, T.; Chmielewski, P. J.; Cybińska, J.; Zafra, J. L.; Casado, J.; Vives, T.; Crassous, J.; Favereau, L.; Stępień, M. Lemniscular [16]Cycloparaphenylene: A Radially Conjugated Figure-Eight Aromatic Molecule. *J. Am. Chem. Soc.* **2019**, *141*, 7421–7427.
(32) Tanaka, K. Rhodium-Mediated [2 + 2 + 2] Cycloaddition. In *Transition-Metal-Mediated Aromatic Ring Construction*; John Wiley & Sons, Ltd, 2013; pp 127–160.
(33) Pla-Quintana, A.; Roglans, A. The Choice of Rhodium Catalysts in [2+2+2] Cycloaddition Reaction: A Personal Account. *Molecules* **2022**, *27*, 1332.
(34) Kumar, P.; Louie, J. Nickel-Mediated [2 + 2 + 2] Cycloaddition. In *Transition-Metal-Mediated Aromatic Ring Construction*; John Wiley & Sons, Ltd, 2013; pp 37–70.
(35) Stará, I. G.; Starý, I.; Kollárovič, A.; Teplý, F.; Vyskočil, Š.; Šaman, D. Transition Metal Catalysed Synthesis of Tetrahydro Derivatives of [5]-, [6]- and [7]Helicene. *Tetrahedron Lett.* **1999**, *40*, 1993–1996.
(36) Teplý, F.; Stará, I. G.; Starý, I.; Kollárovič, A.; Šaman, D.; Rulíšek, L.; Fiedler, P. Synthesis of [5]-, [6]-, and [7]Helicene via Ni(0)- or Co(I)-Catalyzed Isomerization of Aromatic Cis,Cis-Dienetriynes. *J. Am. Chem. Soc.* **2002**, *124*, 9175–9180.
(37) Kotha, S.; Brahmachary, E.; Lahiri, K. Transition Metal Catalyzed [2+2+2] Cycloaddition and Application in Organic Synthesis. *Eur. J. Org. Chem.* **2005**, *2005*, 4741–4767.
(38) Peña, D.; Escudero, S.; Pérez, D.; Guitián, E.; Castedo, L. Efficient Palladium-Catalyzed Cyclotrimerization of Arynes: Synthesis of Triphenylenes. *Angew. Chem. Int. Ed.* **1998**, *37*, 2659–2661.
(39) Peña, D.; Pérez, D.; Guitián, E. Cyclotrimerization Reactions of Arynes and Strained Cycloalkynes. *Chem. Rec.* **2007**, *7*, 326–333.
(40) Colwell, C. E.; Price, T. W.; Stauch, T.; Jasti, R. Strain Visualization for Strained Macrocycles. *Chem. Sci.* **2020**, *11*, 3923–3930.
(41) Adamska, L.; Nayyar, I.; Chen, H.; Swan, A. K.; Oldani, N.; Fernandez-Alberti, S.; Golder, M. R.; Jasti, R.; Doorn, S. K.; Tretiak, S. Self-Trapping of Excitons, Violation of Condon Approximation, and Efficient Fluorescence in Conjugated Cycloparaphenylenes. *Nano Lett.* **2014**, *14*, 6539–6546.
(42) Leonhardt, E. J.; Van Raden, J. M.; Miller, D.; Zakharov, L. N.; Alemán, B.; Jasti, R. A Bottom-Up Approach to Solution-Processed, Atomically Precise Graphitic Cylinders on Graphite. *Nano Lett.* **2018**, *18*, 7991–7997.
(43) Van Raden, J. M.; Leonhardt, E. J.; Zakharov, L. N.; Pérez-Guardiola, A.; Pérez-Jiménez, A. J.; Marshall, C. R.; Brozek, C. K.; Sancho-García, J. C.; Jasti, R. Precision Nanotube Mimics via Self-Assembly of Programmed Carbon Nanohoops. *J. Org. Chem.* **2020**, *85*, 129–141.
(44) Lovell, T. C.; Colwell, C. E.; Zakharov, L. N.; Jasti, R. Symmetry Breaking and the Turn-on Fluorescence of Small, Highly Strained Carbon Nanohoops. *Chem. Sci.* **2019**, *10*, 3786–3790.
(45) Chen, D.; Wada, Y.; Kusakabe, Y.; Sun, L.; Kayahara, E.; Suzuki, K.; Tanaka, H.; Yamago, S.; Kaji, H.; Zysman-Colman, E. A Donor–Acceptor 10-Cycloparaphenylene and Its Use as an Emitter in an Organic Light-Emitting Diode. *Org. Lett.* **2023**, *25*, 998–1002.
(46) Kuwabara, T.; Orii, J.; Segawa, Y.; Itami, K. Curved Oligophenylenes as Donors in Shape-Persistent Donor–Acceptor Macrocycles with Solvatofluorochromic Properties. *Angew. Chem. Int. Ed.* **2015**, *54*, 9646–9649.
(47) Lovell, T. C.; Garrison, Z. R.; Jasti, R. Synthesis, Characterization, and Computational Investigation of Bright Orange-Emitting Benzothiadiazole [10]Cycloparaphenylene. *Angew. Chem. Int. Ed.* **2020**, *59*, 14363–14367.
(48) Pedersen, V. B. R.; Price, T. W.; Kofod, N.; Zakharov, L. N.; Laursen, B. W.; Jasti, R.; Brøndsted Nielsen, M. Synthesis and Properties of Fluorenone-Containing Cycloparaphenylenes and Their Late-Stage Transformation. *Chem. Eur. J.* **2024**, *30*, e202303490.
(49) Barnsley, J. E.; Shillito, G. E.; Mapley, J. I.; Larsen, C. B.; Lucas, N. T.; Gordon, K. C. Walking the Emission Tightrope: Spectral and Computational Analysis of Some Dual-Emitting Benzothiadiazole Donor–Acceptor Dyes. *J. Phys. Chem. A* **2018**, *122*, 7991–8006.
(50) Caspar, J. V.; Meyer, T. J. Application of the Energy Gap Law to Nonradiative, Excited-State Decay. *J. Phys. Chem.* **1983**, *87*, 952–957.